A Wave-Relative Framework Analysis of AEW–MCS Interactions Leading to Tropical Cyclogenesis

KELLY M. NÚÑEZ OCASIO,[a] JENNI L. EVANS,[a] AND GEORGE S. YOUNG[a]

[a] *Department of Meteorology and Atmospheric Science, The Pennsylvania State University, University Park, Pennsylvania*

(Manuscript received 14 May 2020, in final form 17 September 2020)

ABSTRACT: An African easterly wave (AEW) and associated mesoscale convective systems (MCSs) dataset has been created and used to evaluate the propagation of MCSs, AEWs, and, especially, the propagation of MCSs relative to the AEW with which they are associated (i.e., wave-relative framework). The thermodynamic characteristics of AEW–MCS systems are also analyzed. The analysis is done for both AEW–MCS systems that develop into tropical cyclones and those that do not to quantify significant differences. It is shown that developing AEWs over West Africa are associated with a larger number of convective cloud clusters (CCCs; squall-line-type systems) than nondeveloping AEWs. The MCSs of developing AEWs propagate at the same speed of the AEW trough in addition to being in phase with the trough, whereas convection associated with nondeveloping AEWs over West Africa moves faster than the trough and is positioned south of it. These differences become important for the intensification of the AEW vortex as this slower-moving convection (i.e., moving at the same speed of the AEW trough) spends more time supplying moisture and latent heat to the AEW vortex, supporting its further intensification. An analysis of the rainfall rate (MCS intensity), MCS area, and latent heating rate contribution reveals that there are statistically significant differences between developing AEWs and nondeveloping AEWs, especially over West Africa where the fraction of extremely large MCS areas associated with developing AEWs is larger than for nondeveloping AEWs.

KEYWORDS: Africa; Mesoscale systems; Waves, atmospheric; Cyclogenesis/cyclolysis; Latent heating/cooling; Statistics

1. Introduction

In the most recent review of tropical cyclogenesis (Tang et al. 2020) the World Meteorological Organization definition of tropical cyclogenesis is presented: ''the development from a tropical disturbance—'''a discrete tropical. . .weather system of apparently organized convection'—to a tropical depression—'a warm-core, non-frontal, synoptic-scale cyclone with organized deep convection and a closed surface wind circulation about a well-defined center.''' From this definition, organized convection is essential both prior to and after tropical cyclogenesis. Over West Africa and the Atlantic Ocean basin, the interactions between mesoscale convective systems (MCSs) and African easterly waves (AEWs) have been studied in respect to tropical cyclogenesis (TCG).

In an AEW climatology study Hopsch et al. (2010) found that developing AEWs (DAEWs; those that develop into at least a tropical depression) showed stronger low-level circulation, particularly while over high mountains, and were more convectively active than nondeveloping AEWs (NDAEWs). Recently Brammer and Thorncroft (2015) developed an AEW tracking algorithm that uses TCG predictors, yielding results in agreement with Hopsch et al. (2010). They showed that DAEWs experience a moisture ingestion at the lower levels particularly in the northwest quadrant, which aids the AEW in undergoing TCG. Other studies have focused on the evolution of the convection and of the large-scale wave rather than the environment through which the AEW propagates. For example, Leppert et al. (2013) found that the fractional cloud coverage for DAEWs increased as TCG is approached whereas convective intensity (proxied by lightning flash rate) decreased. Their results suggest that convective coverage is more important for TCG than convective intensity. Zawislak and Zipser (2014), using passive microwave data, had similar conclusions as those by Leppert et al. (2013) since they indicate that convective intensity is not a good predictor of tropical cyclogenesis. Semunegus et al. (2017) hypothesize that the strengthening of AEWs is associated with a growth of synoptic-scale MCS activity providing diabatic heating.

While some studies of AEWs have analyzed the role of MCSs in the initiation of the waves (Berry and Thorncroft, 2005; Thorncroft et al. 2008; Hsieh and Cook 2005, 2007; Mekonnen and Rossow 2011, 2018), others have shown the role of MCSs in AEW TCG. Schwendike and Jones (2010) showed that the low-level cyclonic circulation associated with the precursor of Helene was intensified through vortex stretching once a midlevel vorticity anomaly from the convection had moved over the low-level cyclonic circulation. This interaction between a synoptic-scale wave and its embedded MCS(s) was also identified in an analysis of the precursor of Hurricane Alberto (e.g., Lin et al. 2005). Following Lin et al. (2005, 2013), hereinafter these coupled systems will be called AEW–MCS systems.

Tomassini et al. (2017) argue that both the position of moisture and latent heating relative to the AEW trough are essential. Additionally, they say that AEW growth could be explained via moist baroclinic instability. Recently, Adames and Ming (2018) showed that, for synoptic-scale Asian monsoonal disturbances (SMDs), vortex stretching due to convection ahead of the wave trough can cause an acceleration and strengthening of the wave. The SMDs exhibit

Corresponding author: Kelly M. Núñez Ocasio, kmn18@psu.edu

DOI: 10.1175/MWR-D-20-0152.1

similar horizontal scales to AEWs and both have circulation anomalies that are strongest in the lower troposphere. Moreover, through convective-permitting simulations of two AEWs, Russell et al. (2020) showed that AEWs exhibit a moisture instability similar to that presented in Adames and Ming (2018) for SMDs. This instability is driven by the vertical heating of MCSs which produces a region of potential vorticity (PV) anomaly, causing the AEW trough to intensify. Thus, the findings of these studies, suggests that the speed and intensity of the AEW are influenced by the convection.

In using observations to explore the influence of MCSs on the AEW, this work to some extent will put to test these proposed theoretical models. Analyzing the propagation and position of MCSs relative to the AEW they are embedded in could be key to understanding the synoptic-scale and mesoscale interactions that occur during AEW intensification and TCG.

Motivated by these previous studies this work has three goals. The first is to build a dataset of AEW–MCS systems. The second is to use this dataset to evaluate the position and propagation of MCSs and AEWs. This includes an evaluation of the position and propagation of MCSs relative to the AEW they are coupled to. Sets of DAEW–MCS and NDAEW–MCS systems will be compared to identify differences between those systems that develop into at least a tropical depression and those that do not. This evaluation, to a certain degree, will enable a comparison between the results presented here and those documented by Adames and Ming (2018) and Russell et al. (2020). The third goal is to investigate the thermodynamic evolution of DAEW–MCS and NDAEW–MCS systems at different positions over Africa (''East,'' ''Central,'' and ''West''). This will be done using the MCS cloud area, cloud area rain rate (a measure of MCS intensity) and latent heating, all three obtained from satellite-derived MCS tracks from Núñez Ocasio et al. (2020). It is hypothesized in this work that differences between the MCSs associated with NDAEWs and MCSs associated with DAEWs can explain (to some extent) why some AEWs undergo TCG. Moreover, that these differences could lie in the latent heat contribution from the MCSs as suggested by Janiga and Thorncroft (2013). As a consequence, both the speed (i.e., Earth-relative propagation) of the MCS(s) coupled to DAEWs, and the speed(s) of MCS(s) relative to DAEWs, may differ with those of MCSs coupled to NDAEWs. It is proposed that these differences between DAEW–MCS and NDAEW–MCS systems can be detected as early as AEW onset, usually over East Africa.

2. Method

a. Data

A 5-yr August–September climatology of DAEWs and NDAEWs from 2004 to 2008 is used in this study. As we are not trying to detect intraseasonal variability, and the analysis is conducted in a wave-relative framework (convection-relative-to-wave), the sample size will depend on the number of MCSs corresponding to each AEW. Climatologically, AEWs have maximum amplitudes at two locations: to the north of the AEJ at the 925-hPa level (northern track) and south of the AEJ at the 700-hPa level (southern track), that is, the AEJ level (Carlson 1969; Reed et al. 1977; Pytharoulis and Thorncroft 1999; Fink and Reiner 2003; Thorncroft and Hodges 2001). AEWs in the southern track—which are known to foster moist convective systems that can support TCG—are more active during August and September (e.g., Duvel 1990; Thorncroft and Hodges 2001; Hopsch et al. 2007). As suggested by Leppert et al. (2013), strong NDAEWs are those that can be tracked for at least 7 days. A linkage between the convectively active and long-lived nature of NDAEWs can be drawn such that by using these two months the comparison between DAEWs and NDAEWs that were likely to undergo TCG is plausible.

The AEW track data used here are based on the tracking methods of Brammer et al. (2018) with assignment of AEWs that developed into tropical systems (i.e., DAEWs) as in Brammer and Thorncroft (2015). The tracks were created using the National Centers for Environmental Prediction Climate Forecast System Reanalysis, version 2 (CFSR v2; Saha et al. 2010). The AEW tracking is done by analyzing mass-weighted centers across several levels and fields including curvature vorticity at 850, 700, and 500 hPa and relative vorticity at 850 and 700 hPa (Brammer et al. 2018). For the purpose of this study, the track of each AEW is considered up to the time step right before it becomes a tropical depression for DAEWs, and for NDAEWs until termination.

In addition, the European Centre for Medium-Range Weather Forecasts (ECMWF) interim reanalysis (ERA-Interim; Dee et al. 2011) is used to identify the northerly and southerly wind maxima associated with each AEW trough of the AEW track data (details of how the southerly and northerly grid points are identified are described in section 2b). The horizontal grid spacing of ERA-Interim is about 0.7° × 0.7°. Both ERA-Interim and the AEW track data have 6-hourly temporal resolution.

In addition to these two datasets, MCS tracks using the Tracking Algorithm for Mesoscale Convective Systems (TAMS, Núñez Ocasio et al. 2020, hereinafter NO20) are used to associate each AEW with its embedded MCS or MCSs. The 2-hourly data from the Meteosat Second Generation satellite, specifically the infrared band, were used to derive the MCS tracks. These MCSs were tracked using a background flow of 12 m s^{-1}. NO20 show that adding a typical climatology value of the background flow to the position of MCSs being track results in more realistic propagation speeds for MCSs. For MCSs over Africa, the presence of the AEJ controls the mean wind for cell motion, and together with the AEJ, a very active southwesterly monsoon flow provides down shear propagation for the systems. MCS tracks are documented by saving all of the cloud elements (CEs; a convective cloud region as described in NO20) associated with the MCS. Data for each CE include the area and CE-wise rain-rate information (refer to NO20, their Fig. 2). Precipitation metrics for each CE are based on a half-hourly product described in NO20. Latent heating rate q is then calculated as

$$q = \rho l_v A R, \tag{1}$$

where ρ is the density of water (997 kg m^{-3}), l_v is the latent heat of vaporization (2.26×10^6 J kg^{-1}), A is the area of the CE

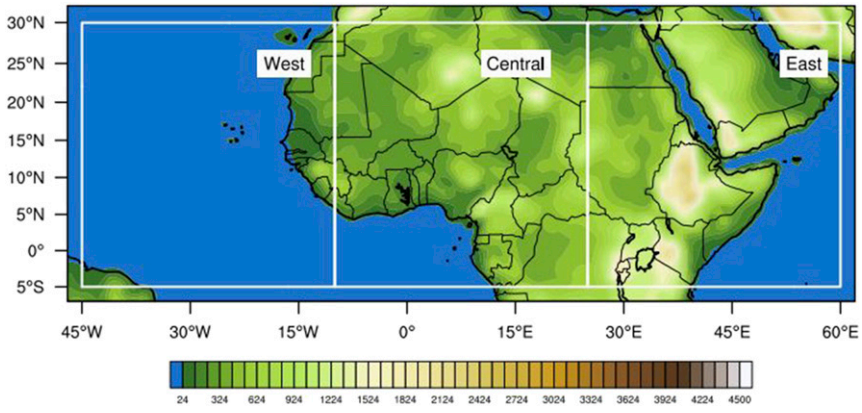

FIG. 1. Elevation map over the domain in the study using ERA-Interim. White boxes denote the regions identified as East, Central, and West Africa.

(m^2), and R is the CE rain rate ($m\,h^{-1}$). Each MCS tracked is classified under one type of a mesoscale convective complex (MCC), convective cloud cluster (CCC), or disorganized long-lived (DLL) system. MCCs are symmetrically organized systems defined by a $\leq$ 235-K brightness temperature region with area $\geq$ 50 000 km^2. Those that are too elliptical to pass the MCC shape are CCCs, and they also fall under organized systems (Evans and Shemo 1996). The DLL category is for systems that do not meet the organized systems area criterion but nonetheless last longer than 6 h (NO20). The domain of study is shown in Fig. 1, spanning latitudes from 5°S to 30°N and longitudes from 45°W to 60°E. The regions denoted by the white boxes are explained in the next section. This large domain is chosen to ensure that both AEWs and MCSs (and consequently AEW–MCS systems) have origins over Africa, off the west coast of Africa, and east and/or east coast of Africa where the Somali jet penetration will modulate the moisture input over the high terrain region and consequently, the convective activity (Vizy and Cook 2003). To exclude AEWs that initiate west of the study domain (e.g., in the western Atlantic Ocean), the position of an AEW trough is checked for the first 48 h of its lifetime.

b. *Identifying the AEW troughs in ERA-Interim*

To examine the AEW–MCS coupled system, the AEW tracks must be supplemented with information on the horizontal structure and evolution of each system. A brief summary of the process is provided here, and a summary of the process for associating MCS with an AEW is provided in section 2c. A more complete description of each approach is provided in the appendix.

To identify each of the CFSRv2-based AEWs in the ERA-Interim, the ERA-Interim meridional wind fields at 850, 700, and 600 hPa are used. First, the closest grid point in the ERA-Interim to the trough center in the AEW track data is located. This grid point becomes the center point of a meridional wind box defined between 5° and 20°N. Initially the box is 2000 km in length based on AEW climatology (e.g., Reed et al. 1977; Burpee, 1974; Kiladis et al. 2009). The meridional wind v in this 2D box is averaged across latitudes and becomes a meridional average. The algorithm then begins to identify grid points for the maximum v (southerly) and minimum v (northerly). To satisfy the typical AEW inverted trough structure, the condition of the southerly being to the east of the northerly must be met. The domain of the meridional average is shrunk until the condition is satisfied. A schematic of this process is shown in Fig. 2 where the blue solid line represents the meridional average. The final southerly and northerly gridpoint location will then be a result of vertically averaging the gridpoint locations obtained at each pressure level.

c. *Associating MCSs with AEWs*

With the use of both the AEW track data and tracks of MCSs over Africa (NO20) an AEW–MCS database is created. To do so, first each AEW trough location is flagged as East, Central, or West as seen from the regions identified in Fig. 1 to analyze the AEW–MCS systems geographically. Those MCSs that are active during the time that a particular AEW is active are identified as first guess candidates for association with that AEW. The largest CE for each MCS at a particular time (mother cloud) is identified to be the one tested for spatial comparison with the AEW. The centroid of this mother cloud must be located between the longitudes of maximum northerly and southerly winds (as identified above) for its MCS to be matched with the AEW trough definitively (Fig. 3). This approach is based on findings by Kiladis et al. (2006) who showed that most of the convective signal coupled to AEWs moves with the trough or ahead. Those MCSs that were matched to an AEW for multiple time steps are used to calculate the speed of the MCS while matched to the AEW, the speed of the AEW while matched to MCS, and the speed of the MCS relative to the AEW to which it is matched (speed of MCS minus speed of the AEW). Note that the speed of MCSs coupled to AEWs calculated is not the instantaneous speed but the average speed of each MCS while coupled to its AEW. Recall that the satellite-derived MCS tracks have 2-h temporal resolution with CE rain information of 30-min resolution matched to the respective MCS time. In this way, a dataset of AEW–MCS systems is created. The appendix includes a more detailed description of the approach.

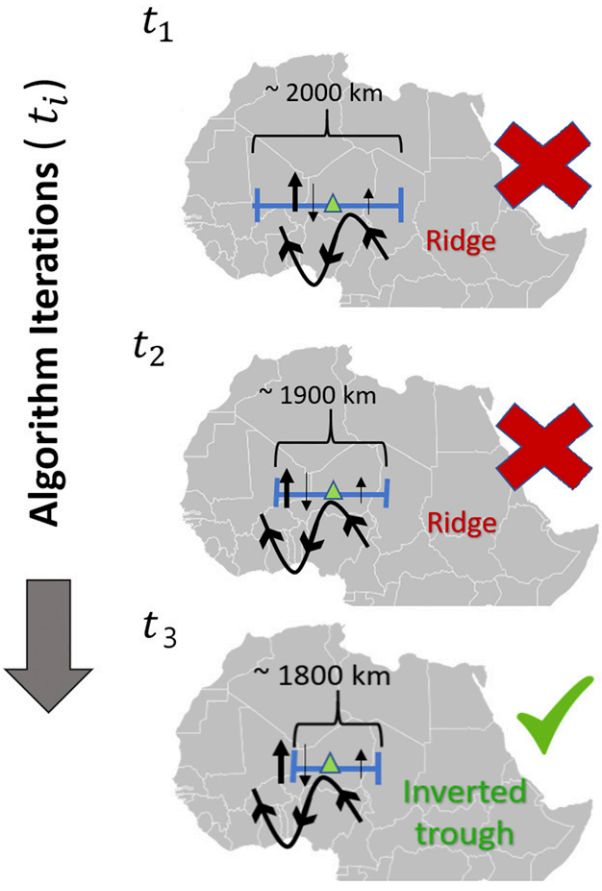

FIG. 2. Schematic diagram depicting how the maximum v (southerly; north-pointing arrows) and minimum v (northerly; south-pointing arrows) associated with the AEW trough are located. The green triangle denotes the center location of the trough, the blue line is the longitudinal span of the meridional average. Algorithm iterations increase from top to bottom. At each iteration, the longitudinal span of the meridional average shrinks longitudinally until the condition of an inverted trough is identified: the maximum southerly grid point being to the east of the maximum northerly grid point. The schematic is not to scale.

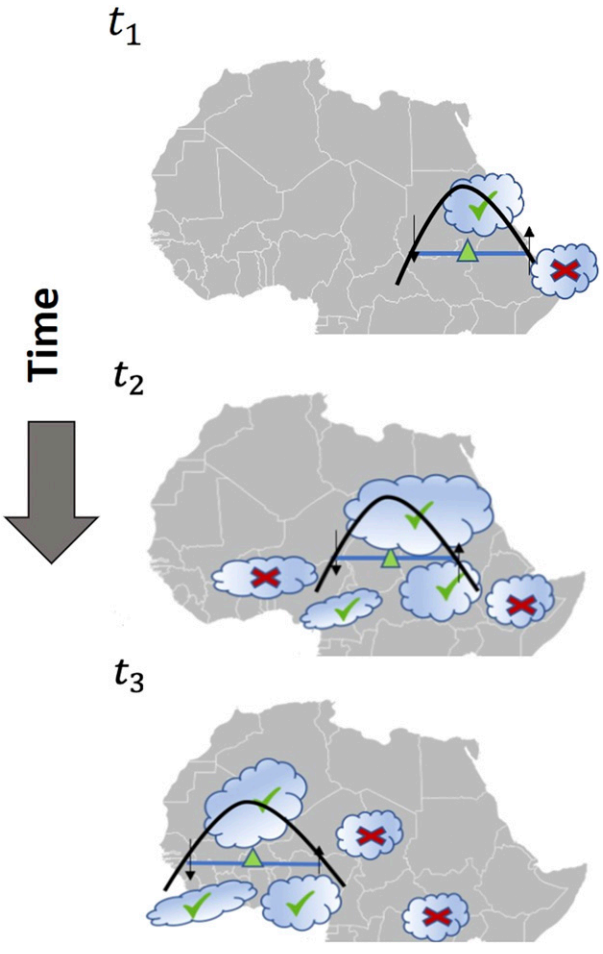

FIG. 3. Schematic diagram depicting how the longitudinal span of the meridional average (blue line) between the southerly (north-pointing arrow) and northerly grid points (trough width/longitudinal extent of the AEW trough) is used to match an AEW with its MCS or MCSs. The solid black line is a representation of the inverted trough; the green triangle is the center location of the AEW trough. CEs with center position marked with a green check mark are chosen to be matched with the AEW, and those with a red cross are not. The schematic is not to scale.

3. Results

The number of DAEWs and NDAEWs broken down by year is shown in Table 1. A breakdown of the population of MCSs (grouped by MCS type) in DAEWs and NDAEWs is shown in Fig. 4. For all three regions and for both DAEWs and NDAEWs, the most common of the MCSs are DLLs. In all cases, CCCs (e.g., squall-line-type systems) are the second largest type group and MCCs are the least common. For both DAEWs and NDAEWs, the total number of MCSs (MCC, CCC and DLL combined) increases from East to West as the AEW evolves. The fraction of DLL does not increase from East to West, although the count does. The number of MCCs increases from East to Central but then drops from Central to West. There is also a decrease in CCCs in each AEW type from East to Central. However, there is an increase of CCCs in DAEWs from Central to West but a decrease of CCCs in NDAEWs.

In prior studies, convection associated with AEWs over eastern Africa had been suggested to evolve with the life stages of the AEW. AEW initiation over East Africa was preceded by a weak and less-organized convective system. Once the disorganized convective event encountered the Ethiopian

TABLE 1. Total number of DAEWs and NDAEWs for the 5-yr climatology from 2004 to 2008 between August and September.

Year	No. of DAEWs	No. of NDAEWs
2004	8	46
2005	5	48
2006	6	31
2007	5	41
2008	3	43

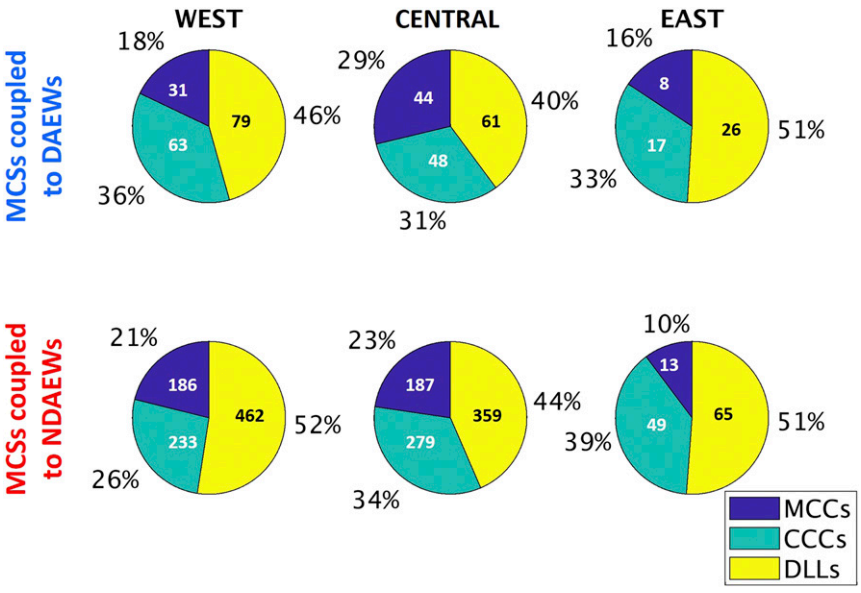

FIG. 4. Pie charts showing the fractions of the population of MCS coupled to DAEWs and NDAEWs that are associated with convection of the type MCC, CCC, and DLL for East, Central, and West Africa.

Highlands where more organized convection is triggered, the AEW came about (Berry and Thorncroft 2005; Mekonnen et al. 2006; Thorncroft et al. 2008; Mekonnen and Rossow 2011). Semunegus et al. (2017) indicated that weak AEWs over East Africa were linked to disorganized convective systems (similar to the definition of DLLs here), while mature AEWs over West Africa have more organized MCS activity. The breakdown presented here shows evidence, however, that AEWs troughs (both of DAEWs and NDAEWs) over East Africa—independent of intensity—also experience the presence of organized convective systems (e.g., CCCs and MCCs) in addition to DLLs. In agreement with the previous studies, over Central Africa both DAEWs and NDAEWs experience a decrease in the number of DLLs (disorganized and short-lived convection) and an increase in MCCs (organized and long-lived convection). Yet another new aspect of this work is the documentation of an increase of CCCs in DAEWs from Central to West but a decrease of CCCs in NDAEWs. It is important to consider MCS type as the influence of an AEW on the convective environment can modulate the growth and type of MCSs associated with the AEW, and this in turn can provide information about the AEW's ability to undergo TCG. Thus, that the DAEWs prefer CCCs (based from the increase in CCC fraction from Central to West) is relevant and is speculated to be related to TCG likelihood. The position and propagation of MCSs relative to DAEWs and NDAEWs over East, Central, and West Africa are compared next, but first the next two paragraphs will explain the types of statistical tests and functions use to present the results in the following subsections.

Results from section 3a will be analyzed by MCS type because it will provide guidance on the type of MCSs coupled to each type of AEW and thus whether TCG is related to the symmetry and spatial scale of the MCSs associated with the wave. In section 3b however, all MCSs are pooled to provide a large sample size for statistical analysis of the convective footprint and sources of variability in the thermodynamic forcing as the AEW evolves.

The majority of the results in sections 3a and 3b are presented using both histograms and kernel density estimates (KDE) on a probability density function (PDF) y-axis. The kernel estimates are nonparametric so as to not make any assumptions of the distribution, and the bandwidth was optimized following Bowman and Azzalini (1997). Although the West, Central, and East regions were all analyzed, the results presented will focus on those regions where the differences between DAEW–MCS and NDAEW–MCS systems were statistically significant. The significance was tested using a two-sided Wilcoxon signed-rank test (hereinafter W; Gibbons and Chakraborti 2011) to test the difference in medians, and a two-sample Kolmogorov–Smirnov test (hereinafter K–S; Massey 1951) to test the differences in distributions. Nonparametric tests were selected over parametric because the distributions are not symmetric and some of the sample sizes are small. The p values obtained from W and K–S tests for the Earth-relative speed of AEWs, Earth-relative speed of MCSs by type and of the wave-relative propagation are reported in Table 2. These will be analyzed more in detail in the following sections.

a. Evaluation of the AEW and MCS position and motion

The estimated distribution of the speed of CCCs coupled to DAEWs (blue) and NDAEWs (red) over East, Central, and West Africa are shown in Fig. 5. Because there were so few CCCs coupled to DAEW over East Africa, the KDEs were not calculated (Fig. 5 East). Over all regions, the distributions of MCSs of both types of AEWs are consistent with typical climatological values with modes between 10 and 13 $m\,s^{-1}$ (e.g.,

TABLE 2. Documentation of significant differences (reported via p values) between speed for each class of convective system when coupled to DAEWs or coupled to NDAEWs. The three columns to the right list the p values for each comparison using the Wilcoxon signed-rank test (first line of each group) and the Kolmogorov–Smirnov test (second line of each group). Comparisons are for the absolute (Earth relative) speed of each type of convection (groups 1–3), and for speed relative to the motion of the wave trough (groups 4–6). The statistical significance of the difference in the absolute speeds of motion for DAEWs and NDAEWs themselves is also evaluated (groups 7–9). The p values in boldface type indicate that the test rejects the null hypothesis at the 5% significance level.

	Tests for differences between DAEWs and NDAEWs	p values: W (above) and K-S (below)		
		West	Central	East
1	MCC Earth-relative speed	0.473	0.204	0.239
		0.149	0.189	0.2118
2	CCC Earth-relative speed	0.237	0.454	1
		0.540	0.713	0.558
3	DLL Earth-relative speed	0.312	0.419	0.850
		0.176	0.524	0.678
4	MCC wave-relative speed	0.062	0.157	0.157
		0.047	0.146	0.212
5	CCC wave-relative speed	**0.009**	0.940	0.660
		0.008	0.274	0.371
6	DLL wave-relative speed	0.674	0.396	0.056
		0.856	0.496	0.1126
7	AEW speed when associated with MCCs	0.051	0.576	0.856
		0.019	0.721	0.920
8	AEW speed when associated with CCCs	0.116	0.343	0.547
		0.280	0.234	0.602
9	AEW speed when associated with DLLs	0.794	0.961	**0.004**
		0.876	0.957	**0.013**

N020; Desbois et al. 1988; Laing et al. 2008; Mathon et al. 2002). There is no statistically significant difference between the distributions or medians of the two groups (see Table 2, group 2, for p values).

Consideration of the wave-relative motion of CCCs over West Africa reveals a clear distinction between DAEWs and NDAEWs (Fig. 6). In Fig. 6, values to the left or right of the zero line represent CCCs moving slower or faster, respectively, than the trough of the wave to which they are coupled. There is a clear tendency for CCCs associated with DAEWs to move at, or just slightly faster than, the speed of its associated DAEW. For NDAEWs the most likely wave-relative speed for CCCs coupled is about 4 m s^{-1}, signifying that the CCCs are moving faster than their associated NDAEW. Interestingly, both W and K-S tests (Fig. 6), indicate statically significant difference between the two groups. To maintain the same phase relationship so as to support further intensification, the CCCs and AEW trough have to be

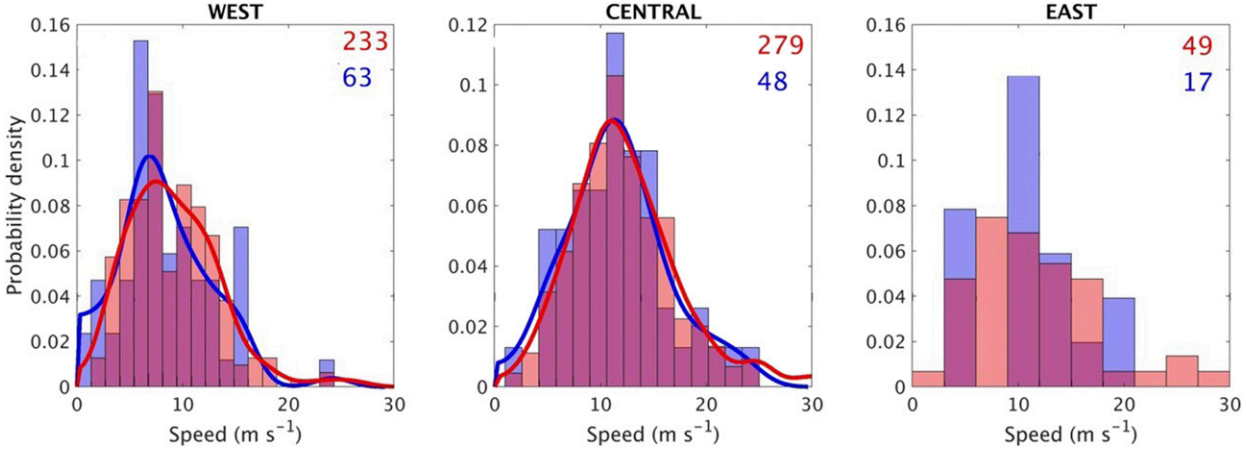

FIG. 5. Kernel density estimates (KDEs) and histograms of the speed of CCCs coupled to DAEWs (blue kernels; lilac colored bars) and NDAEWs (red kernels; adobe colored bars) for East, Central, and West Africa. Purple color in the bars indicates overlap. Sample sizes are given in the top right of each panel. KDEs were not calculated for CCCs coupled to DAEW over East Africa, because of the small sample size.

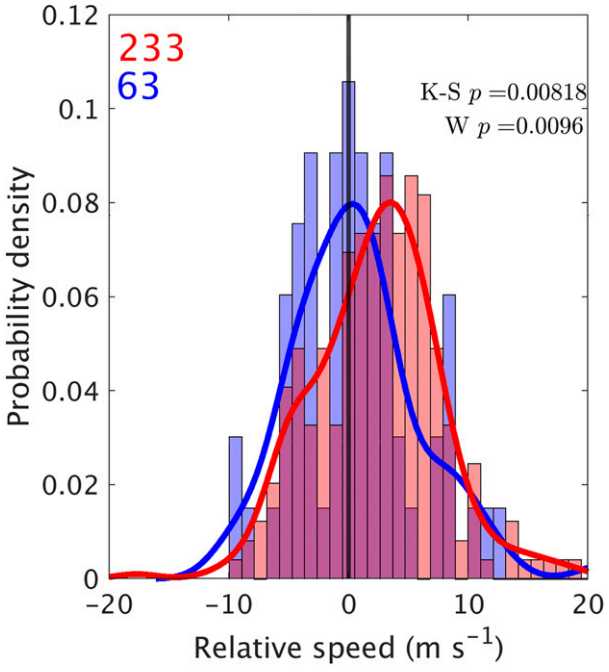

FIG. 6. KDEs and histograms of the CCCs speeds relative to DAEWs (blue kernel; lilac colored bars) and NDAEWs (red kernel; adobe colored bars) for West Africa (i.e., in a wave-relative framework). Purple color in the bars indicates overlap. Sample sizes are given in the top left. The p values for the two tests are shown in the top right and are significant at 5%.

moving at the same speed as is the most likely case here with CCCs coupled to DAEWs.

In agreement with past studies (Kiladis et al. 2006; Fink and Reiner 2003), it is noted that distributions of MCS longitudes relative to DAEW and NDAEW troughs (Fig. 7) reveal that the most probable position of the convection is within the trough (zonally in phase) or ahead (in the northerlies). Is shown in Fig. 7 that the most probable positions are close to the zero line (MCSs at the same longitude as the AEW trough) for all three regions. However, additional insight into the DAEW–MCS and NDAEW–MCS systems is revealed when comparing the differences of the probability distribution of MCSs positions relative to DAEW and NDAEW troughs. Over East Africa, the longitude of MCSs (both organized and disorganized systems) of DAEWs and NDAEWs, is most likely to remain the same as the AEW trough thus, MCSs of both DAEW and NDAEWs are zonally in phase with the trough (Fig. 7, East). Over Central Africa the distributions for the two types of AEWs are statistically significantly different as MCSs of DAEWs are more probable to remain in zonal phase with trough where MCSs of NDAEWs are positioned slightly ahead of the trough (Fig. 7, Central). Once the DAEW–MCS systems transitions to West Africa, the MCSs of DAEW are more likely to move ahead of the trough (northerlies) where the MCSs of NDAEW are more like to be in phase with trough. Up to this point, it has been shown that the MCSs associated with DAEW transition from being zonally in phase with the DAEW trough over East Africa to being zonally out of phase, more likely moving ahead of the trough. This zonal transition of MCSs of DAEWs could explain the distribution of cloud regimes presented in Russell et al. (2020) following Mapes et al. (2006) which describes deep convection in the northerlies with the tail of stratiform cloud in the trough of the AEW. They explain that the PV anomaly generated in the trailing stratiform portion of MCSs moving in the northerlies (west of trough) is what aids the wave growth.

Furthermore, recall from Fig. 6 it is shown that these MCSs positioned in the northerlies over West Africa are more likely moving at the same speed as the AEW trough enabling a phase

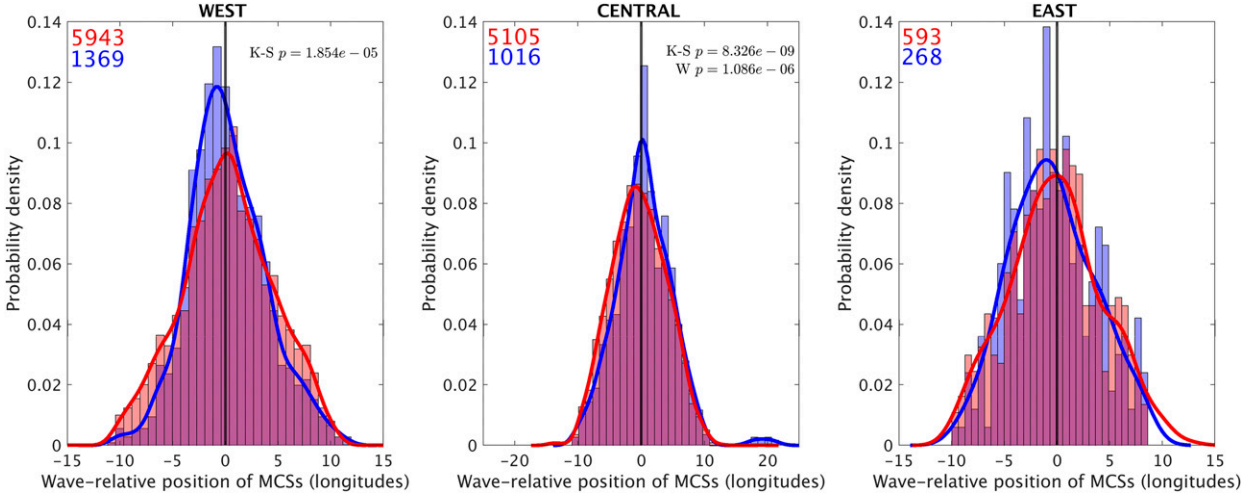

FIG. 7. KDEs and histograms of the MCSs' longitude positions relative to DAEWs (blue kernels; lilac colored bars) and NDAEWs (red kernels; adobe colored bars) for East, Central, and West Africa (i.e., in a wave-relative framework). Purple color in the bars indicates overlap. Sample sizes are given in the top left of each panel. The p values for the two tests are included in the top right of each plot if significant at 5%.

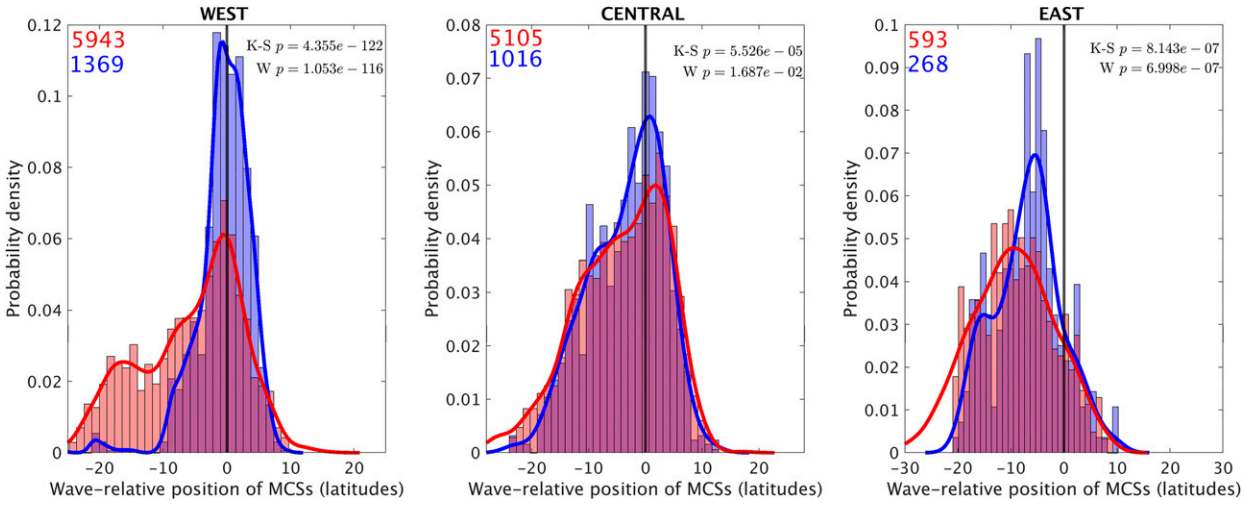

FIG. 8. As in Fig. 7, but for latitude positions.

locking between the northerlies and the MCS, thus supporting the stretched building block hypothesis by Mapes et al. (2006). Still, those MCSs of NDAEWs which are zonally in phase with the trough over West Africa are intensifying the trough through vortex stretching (Adames and Ming 2018). Hence, TCG likelihood based on MCS speed and longitudinal position relative to AEW by themselves cannot fully explain why DAEW–MCS systems undergo TCG while NDAEW–MCS do not. We turn to the probability distributions of MCSs latitudinal position relative to AEW for further analysis.

Figure 8 reveals what could be a significant step toward understanding AEW–MCS interactions and its relation to TCG. It is shown that as early as in AEW onset over East Africa, and right up to the West African coast, MCSs of DAEWs are more likely to move at the same latitude as the DAEW trough (we will call this latitudinal phase locking). However, MCSs of NDAEWs are positioned south of the trough. Note that this is shown by the shift of the NDAEW's distribution to the left of the zero line reflecting MCSs of NDAEWs to be south of the NDAEW's trough (Fig. 8). These results have important implications in our current understanding of TCG. We suggest that CCCs' speed relative to AEW trough over West Africa and the latitudinal phasing between MCSs and AEW trough throughout the whole lifetime are crucial for further intensification of the AEW, and consequently, may be crucial to increasing the potential for TCG in West Africa. Next we present a hypothesis that tries to explain these results.

We hypothesize that the favorable phasing attained by DAEW–MCS systems in this work is due to the combination of an intense AEJ and a strong monsoon trough, both providing a more moist and shear-enhanced environment for the coupled system to grow and propagate. The NDAEWs propagating in a less favorable environment are less likely to couple and become in phase with MCSs as successfully as DAEWs. The result of this is that MCSs of NDAEWs remain south of the NDAEW trough, more likely unable to benefit from any positive feedback by the low-level convergence of the wave trough. This in turn, makes MCSs of NDAEWs more susceptible to midlevel dry air intrusion that results in stronger downdrafts, cold pools, and, hence, faster propagation as seen in the results. Ongoing work seeks to study the position of the DAEWs and NDAEWs relative to the West African monsoon to test this hypothesis. This will aid in understanding whether TCG is likely when DAEW–MCS propagate in a more moist and shear-enhanced environment.

b. *Thermodynamic characteristics of DAEW–MCS and NDAEW–MCS systems*

It is hypothesized that MCSs that are latitudinally in phase and moving at the same speed as the AEW trough (Fig. 6, West) can contribute more latent heat to the AEW vortex—resulting in local generation of potential vorticity in the region of the AEW trough (Schwendike and Jones 2010; Tomassini 2018; Russell et al. 2020)—and support further intensification of the AEW, increasing the likelihood of TCG. Adames and Ming (2018) showed that longer-lasting precipitation results in a larger shift of precipitation toward the center of low pressure, leading to more stretching of vorticity near the center of the trough vortex. Aside of their speed and position relative to the AEW trough, an MCS cannot diabatically force intensification of the DAEW in an unfavorable thermodynamic environment. Barnes and Sieckman (1984) showed that slow-moving convective lines developed in a slightly more favorable thermodynamic environment (higher equivalent potential temperature) than faster-moving lines. Their result then suggests that the slow-moving CCCs coupled to DAEWs (Fig. 6) are evolving in a more thermodynamically favorable environment. To test this idea, the next section will analyze thermodynamic characteristics of the convection coupled to DAEWs and NDAEWs.

Recall that cloud elements are convective cloud regions as described in NO20 associated with the MCS. Figure 9 shows the histograms and KDEs of CE areas for MCSs coupled to DAEWs (blue) and NDAEWs (red) for the three regions. For the three geographic regions and AEW types, the most

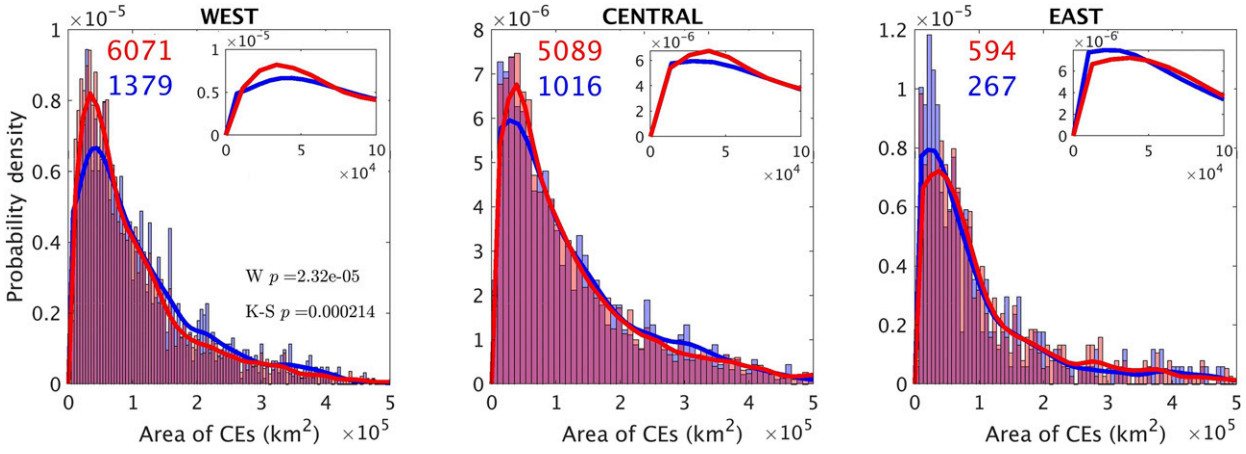

FIG. 9. KDEs and histograms of the area of all CEs' types coupled to DAEWs (blue kernels; lilac colored bars) and NDAEWs (red kernels; adobe colored bars) over East, Central, and West Africa. Purple color in the bars indicates overlap. Sample sizes are given in the top left of each panel. The p values for the two tests are included in each plot if significant at 5%. The top-right inset plots are a zoom in of the KDEs' peaks.

probable area of CEs lies in the range of 0.5×10^5–1×10^5 km^2 with skewness in the range between 2 and 3 and, thus, long right tails. The more extreme areas become more common over West Africa as the distributions show statistically significant difference (Fig. 9 West, W, and K-S tests). Except over East, the fatter tails for CEs coupled to DAEWs indicate higher probabilities of larger areas of MCS convection for DAEWs compared to NDAEWs (red curve). The fraction of areas greater than 2×10^5 km^2 for CEs coupled to DAEWs (NDAEWs) over East, Central, and West Africa are 17% (18%), 22% (21%), and 17% (14%), respectively. The 2×10^5 km^2 threshold is chosen because it is a representative value of the upper 20% (80% quantile) of the population. Using a threshold of 1.5×10^5 km^2—still a characteristic value of large organized convective events—the area fractions for DAEWs (NDAEWs) over East, Central, and West Africa are 24% (26%), 32% (30%), and 26% (21%), respectively. These results agree with Leppert et al. (2013), who showed that over the region of potential TCG (West) the cloud area is significantly greater for DAEWs than for NDAEWs. The work shown here however, shows that in addition, slightly greater CE areas for DAEWs are found over East and Central Africa.

Figure 10 shows the distributions of rain-rate statistics for CEs coupled to DAEWs and NDAEWs for each region. Rain rate is a measure of MCS convective intensity. The mode of the distribution for CE rain-rate median for both groups and three regions lies between 1 and 4 mm h^{-1}. Similar to CEs areas of DAEWs (Fig. 9, blue curve), the MCS intensity measured by the CE rain rate (Fig. 10) shows a tail of higher probabilities for more intense MCSs coupled to DAEWs than to NDAEWs over West and East. The difference between medians of the CE rain-rate median are statistically significant based on W test (Fig. 10, top row West and East).

The distributions for the CE rain-rate skewness for CEs coupled to DAEWs and NDAEWs are plotted in Fig. 10, middle row. Over East Africa, the KDE for CEs coupled to DAEWs is shifted toward the left to the smaller values resulting in a significantly different distribution from that for CEs coupled to NDAEWs. These results suggest that the intensity distribution of the convection within AEWs over East Africa is more symmetrical for DAEWs than for NDAEWs. Once the AEW–MCS systems move into Central Africa, there is not much difference between the two groups. Over West Africa, a further shift to the right of the skewness curve for CEs of DAEWs is evident. The fatter tail of rain-rate standard deviation (Fig. 10, blue curve, West in bottom row) suggests that DAEW convection intensity in this region is more variable than NDAEWs convection. This results in stronger (higher rain rates) and bigger (e.g., NO20) deep convection moving with DAEWs over West Africa than with NDAEWs. The combination of larger CE area and intensity (rain rate) over West Africa should translate to a larger latent heat contribution to the development of DAEWs than is the case for NDAEWs.

The latent heating rate contribution of CEs coupled to DAEWs and NDAEWs is calculated using Eq. (1) (Fig. 11). Although the latent heat rate contribution is not statistically significantly different between groups for East and Central, it is significant in West. Both CE area and rain-rate differences resulted in a larger latent heat rate contribution for DAEWs than for NDAEWs over West Africa as by comparing the tails of the DAEWs and NDAEWs (Fig. 11 West, blue and red kernel curves, respectively). As suggested in the last section and consistent with Janiga and Thorncroft (2013) and Janiga and Thorncroft (2016), these differences in latent heat rate are important for intensification and from these results we suggest that are also important for TCG likelihood. For DAEWs, this implies a gain of energy to the DAEW vortex that eventually undergoes TCG.

c. Variance decomposition for latent heat rate of DAEW–MCS and NDAEW–MCS systems

To quantify which MCS attribute (area or intensity) contributes more to the variability of the latent heat rate of AEW–MCS systems, a variance decomposition is done following Goodman (1960) and Kumpf et al. (2015). The latent

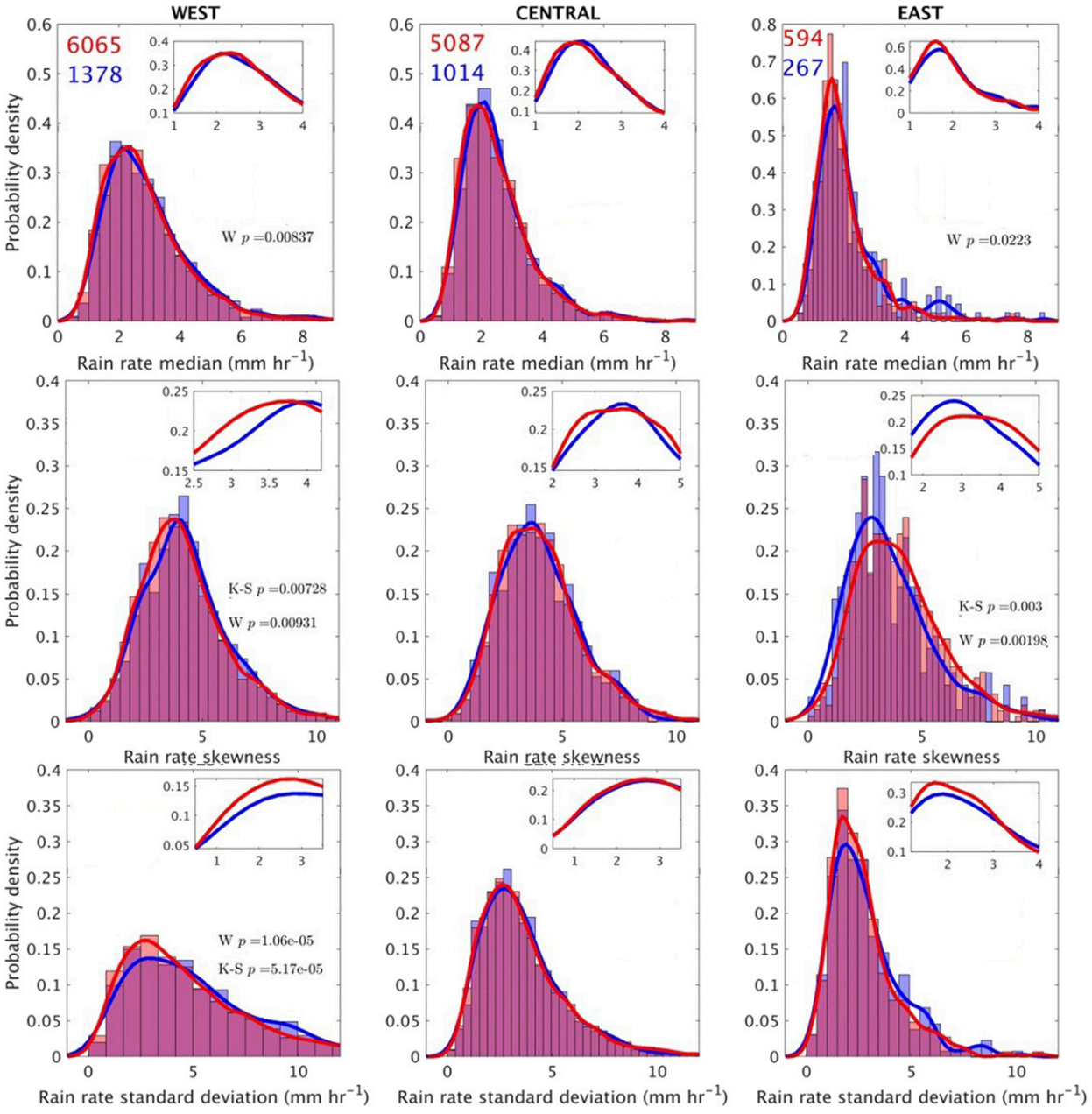

FIG. 10. KDEs and histograms of (top) CE-wise rain-rate median, (middle) CE-wise rain-rate skewness, and (bottom) CE-wise rain-rate standard deviation for MCSs of DAEWs (blue kernels; lilac colored bars) and NDAEWs (red kernels; adobe colored bars) over East, Central, and West Africa. Purple color in the bars indicates overlap. The CE-wise rain-rate data are based on the half-hourly product described in NO20. Sample sizes for each column are given in the top left of each panel in the top row. The p values for the two tests are included in each plot if significant at 5%. The top-right inset plots are a zoom in of the KDEs' peaks.

heating rate q [see Eq. (1)] is proportional to the product of the rain rate R and the CE area A. Partitioning each variable into its mean and perturbation terms allows the variance of latent heat rate to be decomposed as

$$\mathrm{Var}(q) = \overline{(q-\overline{q})^2} = \overline{q'^2} = \overline{R}^2\overline{A'^2} + \overline{A}^2\overline{R'^2} + 2\overline{R}\,\overline{R'A'^2} + 2\overline{A}\,\overline{R'^2A'} + 2\overline{RA}\,\overline{R'A'} + \overline{R'^2A'^2} - \overline{R'A'}^2. \quad (2)$$

Table 3 shows the fractional contribution for each decomposed term in Eq. (2) for DAEWs and NDAEWs. The latent heat variance is expressed in terms of the means and cofluctuations of CE area and rain rate. For both types of waves the first two terms are by far the largest. The first term is the square of the mean rain-rate times the variance of area. The second term is the square of mean area times the variance of rain rate. With a value of 0.650 for DAEWs and of 0.577 for NDAEWs,

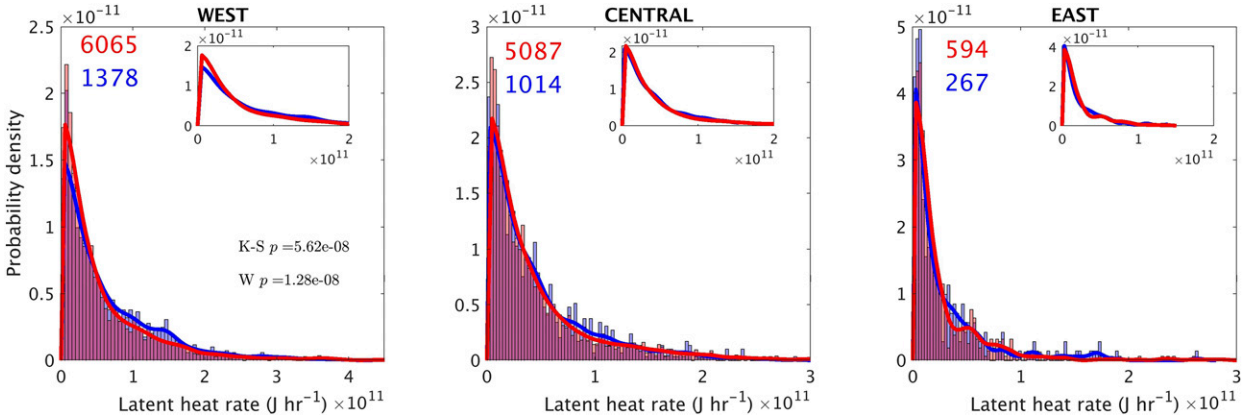

FIG. 11. As in Fig. 10, but for latent heat rate of all CEs coupled to DAEWs (blue kernels; lilac colored bars) and NDAEWs (red kernels; adobe colored bars).

variability of AEW–MCS system area explains more of their latent heating rate variance than does rain-rate variability. These results agree with Leppert et al. (2013), as they proposed that cloud area coverage was more important for undergoing TCG than convection intensity. The main difference between this study and theirs is that convection intensity in their work was measured using lighting flash rate and cloud area using cloud coverage % while in this work the actual CE information for each MCS tracked is used. The rest of the terms in Table 3 contribute less than 30% to the variance of latent heat rate and largely cancel. Next section will summarize and present a conceptual model that builds upon these results.

4. Summary and conceptual model

An AEW–MCS system dataset has been created and used to evaluate the position and propagation of MCSs, AEWs, and especially, the position and propagation of MCSs relative to the AEW they are coupled to (i.e., in the wave-relative framework). This evaluation was done for DAEW–MCS and NDAEW–MCS systems. Results reflect important distinctions that are positively contributing to TCG. It was shown that DAEWs over West Africa are coupled to a larger population of CCC-type convection (which includes squall lines) than NDAEWs. It is important to consider MCS type as the influence of an AEW on the convective environment can modulate the growth and type of MCSs associated with the AEW, and this in turn can provide information about the AEW's ability to undergo TCG. Thus, that the DAEWs prefer CCCs (based on the increase in CCC fraction from Central to West) is relevant and it is speculated to be related to TCG likelihood. The population breakdown of MCSs by type for DAEW–MCS and NDAEW–MCS systems also indicates that both DAEW and NDAEWs over East Africa—independent of intensity—experience the presence of organized convective systems (e.g., CCCs and MCCs) in addition to DLLs.

An analysis of the rainfall rate (a measure of MCS intensity), CE area and latent heat rate contribution, reveals that both the size of the convection and its intensity, are statistically significantly different between DAEWs and NDAEWs, specially over West Africa. Moreover, the fraction of CEs with areas greater than $1.5 \times 10^5\,\mathrm{km}^2$ was higher for DAEWs over Central and West Africa than for NDAEWs. This suggests that MCS area is a better predictor of TCG than MCS intensity consistent with past studies (Leppert et al. 2013; Zawislak and Zipser 2014). A variance decomposition analysis indicates that the contribution of MCS area variability to the latent heat rate variance of AEW–MCS systems is larger than that from rain-rate variance.

We conclude that leading factors over Africa for subsequent TCG can be: 1) the latitudinal phase locking of MCSs with AEW trough–which we show to be the case for DAEWs from the initiating stages over East Africa through to the coast of West Africa—and 2) CCCs maintaining the same propagation speed of the AEW trough. TCG will be favored when MCSs (specifically CCCs over West Africa), move at the same speed as the AEW trough. Maintaining the same speed ensures maintenance of the phase relationship (both latitudinally and longitudinally). Both of these factors were not very likely for NDAEW–MCS systems.

To summarize the analysis presented in this work, a conceptual model is presented in Fig. 12. For DAEW–MCS systems, TCG is favored when CCCs (denoted by the clouds in Fig. 12), independent of the zonal phasing, are latitudinally in

TABLE 3. Values for latent heat rate variance q [Var(q)] and the terms of its decomposition for DAEWs and NDAEWs; R is the rain rate, and A is the CE area.

Type of AEWs	Var(q)	$\overline{R^2}\,\overline{A'^2}$	$\overline{A^2}\,\overline{R'^2}$	$2\overline{R}\,\overline{R'A'^2}$	$2\overline{A}\,\overline{R'^2A'}$	$\overline{2RA}\,\overline{R'A'}$	$\overline{R'^2A'^2}$	$-\overline{R'A'}^2$
DAEWs	9.472×10^8	0.650	0.369	−0.0626	−0.171	0.0422	0.171	-4.839×10^{-4}
NDAEWs	9.164×10^8	0.577	0.279	0.0228	−0.101	0.0651	0.1579	−0.0015

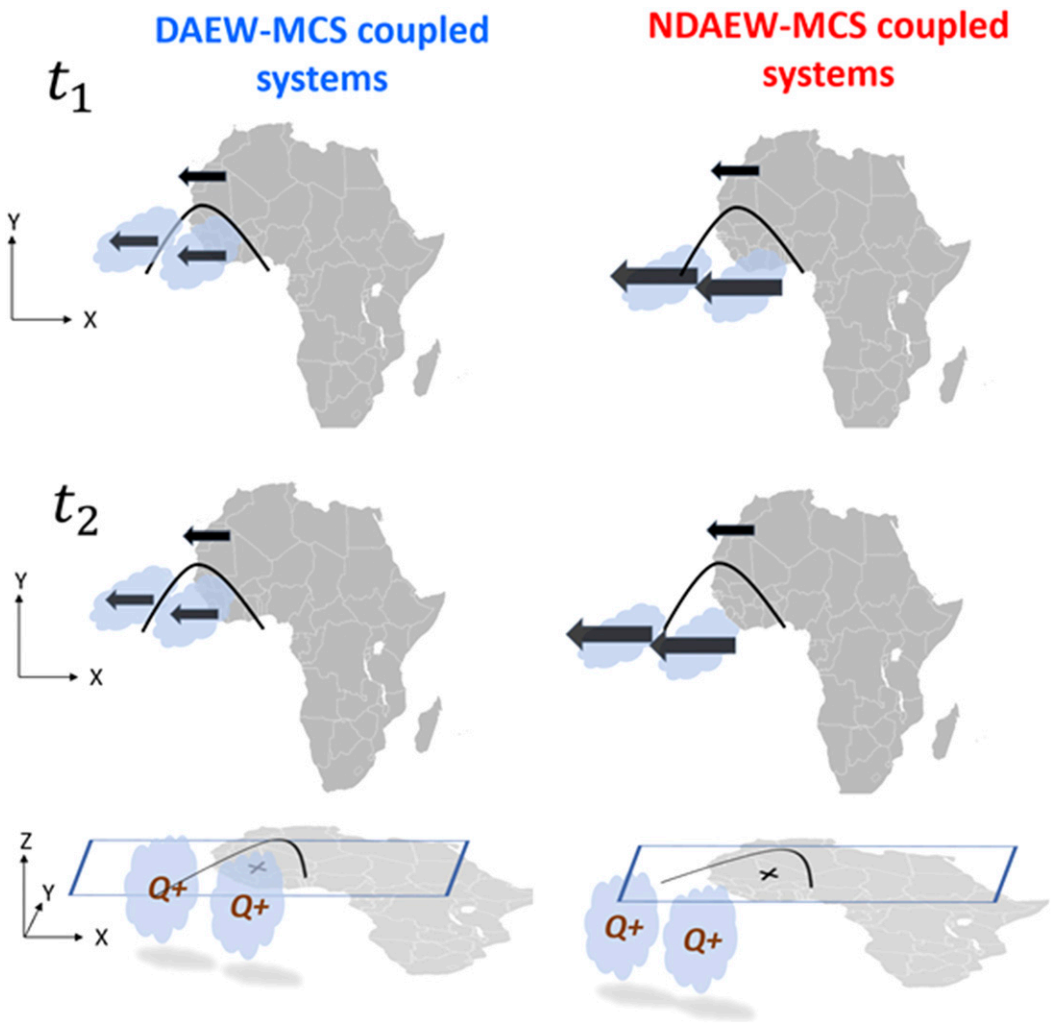

FIG. 12. Conceptual model describing how the chances of TCG increase with appropriate convective coupling. For DAEW–MCS systems, TCG is favored when CCCs (denoted by the cloud) move at the same speed as the AEW trough (direction and magnitude of propagation are denoted by solid black arrows) and are latitudinally in phase with the trough. Maintaining the same speed insures the same phase relationship. Note that convection of NDAEWs is positioned south of the trough and propagates faster than the trough; thus, phase locking and further intensification are less likely.

phase with the AEW. Notice how CCCs of the DAEW are located at the same latitude as the DAEW trough whereas CCCs of the NDAEW are further south of the trough. TCG is even more favored when the latitudinal phase locking between the AEW trough and the convection is maintained by the convection moving at the same speed as the AEW trough. We see this in Fig. 12 as in t_2 convection remains in the same phase with the DAEW trough whereas convection of NDAEWs now is out of phase as it moves faster than the trough. This latitudinal phase locking between MCSs and DAEW is associated with AEW vortex intensification. Following Adames and Ming (2018), Russell et al. (2020), and Tomassini et al. (2017), latent heating will be enclosed in the AEW vortex which promotes stretching of the vortex and thus, further intensification. Since the CCCs remain in phase with the DAEW trough (both latitudinally and longitudinally) they will spend more time supplying energy to the synoptic-scale vortex. In contrast, for NDAEWs the heating is misused as the CCCs not only outrun the trough but also lie south of AEW vortex. These results provide observational evidence that both propagation and phasing between MCSs and the AEW they are coupled to are attributes that play a role in TCG likelihood. Tomassini et al. (2017) suspected this in their work studying AEWs. To some extent these results also support the moist instability described by Adames and Ming (2018) for SMDs and by Russell et al. (2020) for AEWs.

We hypothesize that the favorable phasing attained by DAEW–MCS systems in this work is due to the combination of an intense AEJ and a strong monsoon trough, both providing a more moist and shear-enhanced environment for the coupled system to grow and propagate. The NDAEWs propagating in a less favorable environment are less likely to couple and become

in phase with MCSs as successfully as DAEWs. The result of this is that MCSs of NDAEWs remain south of the NDAEW trough, more likely unable to benefit from any positive feedback by the low-level convergence of the wave trough. This in turn, makes MCSs of NDAEWs more susceptible to midlevel dry air intrusion which results in stronger downdrafts, cold pools and, hence, faster propagation as seen in the results.

Ongoing work seeks to study the position of the DAEWs and NDAEWs relative to the West African monsoon to test this hypothesis. This will aid in understanding if TCG is likely when DAEW–MCS propagate in a more moist and shear-enhanced environment. Furthermore, because these results suggest that some DAEWs become potential candidates to undergo subsequent TCG as early as when the trough is still over East Africa—where favorable convective coupling is attained—we suspect that the DAEWs could have some type of ''memory'' as they are developed to be more sustained structures from the start. Ongoing work comparing the environment of DAEWs and NDAEWs over east and west Africa could support this idea and agrees with Barnes and Sieckman (1984) in which these slower moving convective lines that move with the DAEW troughs, exist in a more favorable thermodynamic environment with higher equivalent potential temperature over East Africa and higher CAPE compared to the environment of NDAEWs over East Africa. Analysis of the evolution of AEW structure in response to MCS behavior is a major undertaking, beyond the scope of this paper, but should be addressed in future work.

Acknowledgments. The authors thank Chris Thorncroft, Ron McTaggart-Cowan, Zachary Moon, James Russell, and, especially, Angel Adames, for discussions that helped to inform this study. Thanks are given to Alan Brammer for providing the AEW track data. We thank ECMWF for free access to the ERA-Interim reanalysis data. The feedback by scientists and colleagues at the 2019 Cyclone Workshop and the 100th American Meteorological Society Annual Meeting was also very helpful. The analyses developed here were performed on the Penn State Institute for Computational and Data Sciences Advanced Cyber Infrastructure (ICDS-ACI). This project has received funding from National Oceanic and Atmospheric Administration Educational Partnership Program under Agreement NA16SEC4810006-NCAS-M.

Data availability statement. The AEW–MCS dataset is publicly available and can be found through the Pennsylvania State Data Commons (https://doi.org/10.26208/frz9-7 t95) as well as the TAMS dataset (https://doi.org/10.26208/saxc-fa63).

APPENDIX

Extended Details for the Method

a. *Identifying the AEW troughs in ERA-Interim*

The following steps describe how AEW tracks are identified in ERA-Interim using the meridional wind fields at levels 850, 700 and 600 hPa:

1) The closest grid point in the ERA-Interim grid to the location of each AEW trough center given by the AEW track data is determined.
2) This ERA-Interim grid point is used as the center point of a box using the meridional wind field between 5° and 20°N. This box region is selected so as to capture both north (15°–20°N) and south (5°–15°N) AEW tracks (e.g., Reed et al. 1977; Thorncroft and Hodges, 2001; Fink and Reiner, 2003; Hodges et al. 2003). Initially, it is approximately 2000 km long in the east–west direction; 2000 km is chosen as a first guess of the longitudinal extension of the trough given that the typical AEW wavelength is between 2000 and 4000 km (e.g., Reed et al. 1977; Burpee 1974; Kiladis et al. 2009).
3) Next, the v component of the wind in the 2D box is averaged across latitudes to create a meridional average. Within this meridional average, the grid points of the maximum v (southerly) and minimum v (northerly) associated with the trough are located. The schematic of this process is shown in Fig. 2. The interpretation is as follows. Typically, AEWs have inverted troughs, and, because of that, the southerly grid point must be to the east of the northerly one. At the first iteration in Fig. 2, the maximum (southerly) and minimum v (northerly) do not meet the inverted trough condition because the maximum southerly grid point is to the west of the maximum northerly (thus identifying a ridge rather than the desired trough). At the second iteration, the longitudinal span of the meridional average is shrunk by one grid point at each end. Still, a ridge is identified. In the third iteration, the span is shrunk once again and this time the trough seeking algorithm is successful, because now the maximum v and minimum v grid points satisfy the inverted trough condition. In this way the AEW trough can be identified while allowing for possible asymmetry.
4) The previous steps are done for three different levels (850, 700, and 600 hPa). The final southerly and northerly gridpoint locations will then be a result of vertically averaging the gridpoint locations obtained at each level. This vertical average approach follows Brammer et al. (2018). An additional step is done to guarantee that the longitudinal extent of the trough identified by the southerly and northerly grid points is large enough that is not just a mesoscale feature. Specifically, the longitudinal extent of trough is checked to be greater than one eighth of the original half-trough width being tested (about 2000 km).
5) If, by any chance, the northerly and southerly points cannot be identified for consecutive time steps, or if the identified points are so close to each other that they are not related to a synoptic-scale feature, a cubic spline interpolation is done to ensure that each time step has corresponding southerly and northerly locations. This type of interpolation requires at least four points and is based on a continuity of C^2 (Schoenberg 1946). The zonal distance between the southerly and northerly grid points (the longitudinal extent of the AEW trough/trough width) is important when associating an AEW with its MCSs, which is described in the next section.

b. *Associating MCSs with AEWs*

Having both AEW track data and tracks of MCSs over Africa (NO20), one can develop an AEW–MCS database.

The AEW track data are linearly interpolated in time to increase the original 6-hourly temporal resolution to a 2-hourly temporal resolution for compatibility with the satellite-tracked MCS dataset. Steps used for matching/associating and MCS(s) to AEWs follow:

1) To analyze the spatial and temporal evolution of AEW–MCS systems, at each AEW time step, the location of the AEW trough center is flagged as ''East,'' ''Central,'' or ''West'' as seen from the regions identified in Fig. 1. Those MCSs that are active during the time that a particular AEW is active are identified as first guess candidates for association with that AEW. Because one MCS track may have several CEs at a particular time (from splits and/or mergers), the largest CE (i.e, the ''mother cloud'') for a particular time is identified to be the one tested for spatial comparison with the AEW. The use of the mother cloud is done to ensure that the CE being tested to be matched with an AEW is the most convective cloud and not a trailing small cloud that although propagating with the mother cloud as part of the same MCS, it may diverge from the main convective cloud in the next time frame.
2) The spatial comparison between the mother cloud of the MCS candidate to be matched with an AEW is done next. The centroid of the mother cloud must be located between the longitudes of maximum northerly and southerly winds (as identified above) for its MCS to be matched with the AEW definitively (Fig. 3). This approach is based on findings of Kiladis et al. (2006) who used outgoing longwave radiation measurements, to show that most of the time the convective signal coupled to AEWs moves with the trough or ahead (and thus northerlies) as the AEW moves west and into the Atlantic Ocean region. Other studies have shown similar results (e.g., Cifelli et al. 2010; Fink and Reiner 2003).
3) Those MCSs that were matched to an AEW for multiple time steps are used to calculate the speed of the MCS while matched to the AEW, the speed of the AEW while matched to MCS, and the speed of the MCS relative to the AEW to which it is matched (speed of MCS minus speed of the AEW). Note the speed of MCSs coupled to AEWs calculated is not the instantaneous speed but the average speed of each MCS while coupled to its AEW. In this way, a dataset of AEW–MCS systems is created.

REFERENCES

Adames, A. F., and Y. Ming, 2018: Interactions between water vapor and potential vorticity in synoptic-scale monsoonal disturbances: Moisture vortex instability. *J. Atmos. Sci.*, **75**, 2083–2106, https://doi.org/10.1175/JAS-D-17-0310.1.

Barnes, G. M., and K. Sieckman, 1984: The environment of fast- and slow-moving tropical mesoscale convective cloud lines. *Mon. Wea. Rev.*, **112**, 1782–1794, https://doi.org/10.1175/1520-0493(1984)112<1782:TEOFAS>2.0.CO;2.

Berry, G. J., and C. Thorncroft, 2005: Case study of an intense African easterly wave. *Mon. Wea. Rev.*, **133**, 752–766, https://doi.org/10.1175/MWR2884.1.

Bowman, A., and A. Azzalini, 1997: *Applied Smoothing Techniques for Data Analysis: The Kernel Approach with S-Plus Illustrations*. Oxford Statistical Science Series, Vol 18, Oxford University Press, 204 pp.

Brammer, A., and C. D. Thorncroft, 2015: Variability and evolution of African easterly wave structures and their relationship with tropical cyclogenesis over the eastern Atlantic. *Mon. Wea. Rev.*, **143**, 4975–4995, https://doi.org/10.1175/MWR-D-15-0106.1.

——, ——, and J. P. Dunion, 2018: Observations and predictability of a nondeveloping tropical disturbance over the eastern Atlantic. *Mon. Wea. Rev.*, **146**, 3079–3096, https://doi.org/10.1175/MWR-D-18-0065.1.

Burpee, R. W., 1974: Characteristics of North African easterly waves during the summers of 1968 and 1969. *J. Atmos. Sci.*, **31**, 1556–1570, https://doi.org/10.1175/1520-0469(1974)031<1556:CONAEW>2.0.CO;2.

Carlson, T. N., 1969: Some remarks on African disturbances and their progress over the tropical Atlantic. *Mon. Wea. Rev.*, **97**, 716–726, https://doi.org/10.1175/1520-0493(1969)097<0716:SROADA>2.3.CO;2.

Cifelli, R., T. Lang, S. A. Rutledge, N. Guy, E. J. Zipser, J. Zawislak, and R. Holzworth, 2010: Characteristics of an African easterly wave observed during NAMMA. *J. Atmos. Sci.*, **67**, 3–25, https://doi.org/10.1175/2009JAS3141.1.

Dee, D. P., and Coauthors, 2011: The ERA-Interim reanalysis: Configuration and performance of the data assimilation system. *Quart. J. Roy. Meteor. Soc.*, **137**, 553–597, https://doi.org/10.1002/qj.828.

Desbois, M., T. Kayiranga, B. Gnamien, S. Guessous, and L. Picon, 1988: Characterization of some elements of the Sahelian climate and their interannual variations for July 1983, 1984 and 1985 from the analysis of METEOSAT ISCCP data. *J. Climate*, **1**, 867–904, https://doi.org/10.1175/1520-0442(1988)001<0867:COSEOT>2.0.CO;2.

Duvel, J. P., 1990: Convection over tropical Africa and the Atlantic Ocean during northern summer. Part II: Modulation by easterly waves. *Mon. Wea. Rev.*, **118**, 1855–1868, https://doi.org/10.1175/1520-0493(1990)118<1855:COTAAT>2.0.CO;2.

Evans, J. L., and R. E. Shemo, 1996: A procedure for automated satellite-based identification and climatology development of various classes of organized convection. *J. Appl. Meteor.*, **35**, 638–652, https://doi.org/10.1175/1520-0450(1996)035<0638:APFASB>2.0.CO;2.

Fink, A. H., and A. Reiner, 2003: Spatiotemporal variability of the relation between African easterly waves and West African squall lines in 1998 and 1999. *J. Geophys. Res.*, **108**, 4332, https://doi.org/10.1029/2002JD002816.

Gibbons, J. D., and S. Chakraborti, 2011: Nonparametric statistical inference. *International Encyclopedia of Statistical Science*, M. Lovric, Ed., Springer, 977–979.

Goodman, L. A., 1960: On the exact variance of products. *J. Amer. Stat. Assoc.*, **55**, 708–713, https://doi.org/10.1080/01621459.1960.10483369.

Hodges, K. I., B. J. Hoskins, J. Boyle, and C. Thorncroft, 2003: A comparison of recent reanalysis datasets using objective feature tracking: Storm tracks and tropical easterly waves. *Mon. Wea. Rev.*, **131**, 2012–2037, https://doi.org/10.1175/1520-0493(2003)131<2012:ACORRD>2.0.CO;2.

Hopsch, S. B., C. D. Thorncroft, K. Hodges, and A. Aiyyer, 2007: West African storm tracks and their relationship to Atlantic tropical cyclones. *J. Climate*, **20**, 2468–2483, https://doi.org/10.1175/JCLI4139.1.

——, ——, and K. R. Tyle, 2010: Analysis of African easterly wave structures and their role in influencing tropical cyclogenesis.

Mon. Wea. Rev., **138**, 1399–1419, https://doi.org/10.1175/2009MWR2760.1.

Hsieh, J.-S., and K. H. Cook, 2005: Generation of African easterly wave disturbances: Relationship to the African easterly jet. *Mon. Wea. Rev.*, **133**, 1311–1327, https://doi.org/10.1175/MWR2916.1.

——, and ——, 2007: A study of the energetics of African easterly waves using a regional climate model. *J. Atmos. Sci.*, **64**, 421–440, https://doi.org/10.1175/JAS3851.1.

Janiga, M. A., and C. D. Thorncroft, 2013: Regional differences in the kinematic and thermodynamic structure of African easterly waves. *Quart. J. Roy. Meteor. Soc.*, **139**, 1598–1614, https://doi.org/10.1002/qj.2047.

——, and ——, 2016: The influence of African easterly waves on convection over tropical Africa and the east Atlantic. *Mon. Wea. Rev.*, **144**, 171–192, https://doi.org/10.1175/MWR-D-14-00419.1.

Kiladis, G. N., C. D. Thorncroft, and N. M. J. Hall, 2006: Three-dimensional structure and dynamics of African easterly waves. Part I: Observations. *J. Atmos. Sci.*, **63**, 2212–2230, https://doi.org/10.1175/JAS3741.1.

——, M. C. Wheeler, P. T. Haertel, K. H. Straub, and P. E. Roundy, 2009: Convectively coupled equatorial waves. *Rev. Geophys.*, **47**, RG2003, https://doi.org/10.1029/2008RG000266.

Kumpf, K., S. Blumsack, G. S. Young, and J. R. Brownson, 2015: Portfolio analysis of solar photovoltaics: Quantifying the contributions of locational marginal pricing and power on revenue variability. *Sol. Energy*, **119**, 277–285, https://doi.org/10.1016/j.solener.2015.06.008.

Laing, A. G., R. Carbone, V. Levizzani, and J. Tuttle, 2008: The propagation and diurnal cycles of deep convection in northern tropical Africa. *Quart. J. Roy. Meteor. Soc.*, **134**, 93–109, https://doi.org/10.1002/qj.194.

Leppert, K. D., D. J. Cecil, and W. A. Petersen, 2013: Relation between tropical easterly waves, convection, and tropical cyclogenesis: A Lagrangian perspective. *Mon. Wea. Rev.*, **141**, 2649–2668, https://doi.org/10.1175/MWR-D-12-00217.1.

Lin, Y.-L., K. E. Robertson, and C. M. Hill, 2005: Origin and propagation of a disturbance associated with an African easterly wave as a precursor of hurricane Alberto (2000). *Mon. Wea. Rev.*, **133**, 3276–3298, https://doi.org/10.1175/MWR3035.1.

——, L. Liu, G. Tang, J. Spinks, and W. Jones, 2013: Origin of the pre-tropical storm Debby (2006) African easterly wave-mesoscale convective system. *Meteor. Atmos. Phys.*, **120**, 123–144, https://doi.org/10.1007/s00703-013-0248-6.

Mapes, B., S. Tulich, J. Lin, and P. Zuidema, 2006: The mesoscale convection life cycle: Building block or prototype for large-scale tropical waves? *Dyn. Atmos. Oceans*, **42**, 3–29, https://doi.org/10.1016/j.dynatmoce.2006.03.003.

Massey, F., 1951: The Kolmogorov–Smirnov test for goodness of fit. *J. Amer. Stat. Assoc.*, **46**, 68–78, https://doi.org/10.1080/01621459.1951.10500769.

Mathon, V., H. Laurent, and T. Lebel, 2002: Mesoscale convective system rainfall in the Sahel. *J. Appl. Meteor.*, **41**, 1081–1092, https://doi.org/10.1175/1520-0450(2002)041<1081:MCSRIT>2.0.CO;2.

Mekonnen, A., and W. B. Rossow, 2011: The interaction between deep convection and easterly waves over tropical North Africa: A weather state perspective. *J. Climate*, **24**, 4276–4294, https://doi.org/10.1175/2011JCLI3900.1.

——, and ——, 2018: The interaction between deep convection and easterly wave activity over Africa: Convective transitions and mechanisms. *Mon. Wea. Rev.*, **146**, 1945–1961, https://doi.org/10.1175/MWR-D-17-0217.1.

——, C. D. Thorncroft, and A. R. Aiyyer, 2006: Analysis of convection and its association with African easterly waves. *J. Climate*, **19**, 5405–5421, https://doi.org/10.1175/JCLI3920.1.

Núñez Ocasio, K. M., J. L. Evans, and G. S. Young, 2020: Tracking mesoscale convective systems that are potential candidates for tropical cyclogenesis. *Mon. Wea. Rev.*, **148**, 655–669, https://doi.org/10.1175/MWR-D-19-0070.1.

Pytharoulis, I., and C. Thorncroft, 1999: The low-level structure of African easterly waves in 1995. *Mon. Wea. Rev.*, **127**, 2266–2280, https://doi.org/10.1175/1520-0493(1999)127<2266:TLLSOA>2.0.CO;2.

Reed, R. J., D. C. Norquist, and E. E. Recker, 1977: The structure and properties of African wave disturbances as observed during Phase III of GATE. *Mon. Wea. Rev.*, **105**, 317–333, https://doi.org/10.1175/1520-0493(1977)105<0317:TSAPOA>2.0.CO;2.

Russell, J. O. H., A. Aiyyer, and J. Dylan White, 2020: African easterly wave dynamics in convection-permitting simulations: Rotational stratiform instability as a conceptual model. *J. Adv. Model. Earth Syst.*, **12**, e2019MS001706, https://doi.org/10.1029/2019MS001706.

Saha, S., and Coauthors, 2010: The NCEP Climate Forecast System Reanalysis. *Bull. Amer. Meteor. Soc.*, **91**, 1015–1058, https://doi.org/10.1175/2010BAMS3001.1.

Schoenberg, I. J., 1946: Contributions to the problem of approximation of equidistant data by analytic functions. Part A. On the problem of smoothing or graduation: A first class of analytic approximation formulae. *Quart. Appl. Math.*, **4**, 45–99, https://doi.org/10.1090/qam/15914.

Schwendike, J., and S. C. Jones, 2010: Convection in an African easterly wave over West Africa and the eastern Atlantic: A model case study of Helene (2006). *Quart. J. Roy. Meteor. Soc.*, **136**, 364–396, https://doi.org/10.1002/qj.566.

Semunegus, H., A. Mekonnen, and C. J. Schreck III, 2017: Characterization of convective systems and their association with African easterly waves. *Int. J. Climatol.*, **37**, 4486–4492, https://doi.org/10.1002/joc.5085.

Tang, B. H., and Coauthors, 2020: Recent advances in research on tropical cyclogenesis. *Trop. Cyclone Res. Rev.*, **9**, 87–105, https://doi.org/10.1016/j.tcrr.2020.04.004.

Thorncroft, C. D., and K. Hodges, 2001: African easterly wave variability and its relationship to Atlantic tropical cyclone activity. *J. Climate*, **14**, 1166–1179, https://doi.org/10.1175/1520-0442(2001)014<1166:AEWVAI>2.0.CO;2.

——, N. M. J. Hall, and G. N. Kiladis, 2008: Three-dimensional structure and dynamics of African easterly waves. Part III: Genesis. *J. Atmos. Sci.*, **65**, 3596–3607, https://doi.org/10.1175/2008JAS2575.1.

Tomassini, L., 2018: Mesoscale circulations and organized convection in African easterly waves. *J. Atmos. Sci.*, **75**, 4357–4381, https://doi.org/10.1175/JAS-D-18-0183.1.

——, D. J. Parker, A. Stirling, C. Bain, C. Senior, and S. Milton, 2017: The interaction between moist diabatic processes and the atmospheric circulation in African easterly wave propagation. *Quart. J. Roy. Meteor. Soc.*, **143**, 3207–3227, https://doi.org/10.1002/qj.3173.

Vizy, E. K., and K. H. Cook, 2003: Connections between the summer east African and Indian rainfall regimes. *J. Geophys. Res.*, **108**, 4510, https://doi.org/10.1029/2003JD003452.

Zawislak, J., and E. J. Zipser, 2014: A multisatellite investigation of the convective properties of developing and nondeveloping tropical disturbances. *Mon. Wea. Rev.*, **142**, 4624–4645, https://doi.org/10.1175/MWR-D-14-00028.1.